

End-to-End Alignment of Nanorods in Thin Films

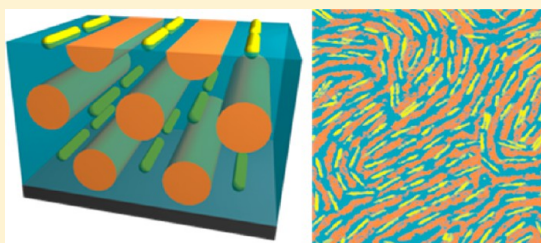
Kari Thorkelsson,[†] James H. Nelson,^{‡,||} A. Paul Alivisatos,^{‡,§} and Ting Xu^{*,†,‡,§}

[†]Department of Materials Science and Engineering and [‡]Department of Chemistry, University of California, Berkeley, California, United States

[§]Materials Sciences Division, Lawrence Berkeley National Laboratory, Berkeley, California, United States

S Supporting Information

ABSTRACT: A simple approach to obtain end-to-end assemblies of nanorods over macroscopic distances in thin films is described. Nanorods with aspect ratio of 8–12 can be aligned parallel to the surface in an end-to-end fashion by imposing geometric confinement via block copolymer-based supramolecular assemblies. Successful control over the orientation and location of nanorods requires a balance of particle–particle interactions and entropy associated with geometric confinement from the supramolecular framework, as well as consideration of the kinetics of assembly.



KEYWORDS: Nanorods, block copolymer-based supramolecule, end-to-end assembly, geometric confinement

Thin films of metallic or semiconducting nanorods (NRs) are a critical component in the fabrication of NR-based nanodevices ranging from photovoltaics,^{1,2} plasmonics,^{3,4} and sensors.^{5,6} Controlling the inter-rod ordering and the macroscopic alignment of NRs in thin films is requisite to access properties unique to NR clusters and to optimize macroscopic responses from the anisotropic properties of NRs.^{5,7} External fields have been extensively used to this end, including controlled drying^{8–11} and electric,¹² magnetic,^{13–15} and shear fields.¹⁶ There has been much success in obtaining ordered arrays of NRs where the macroscopically aligned NRs are arranged side-to-side. For many applications such as light harvesting, side-to-side assembly of NRs is desirable.^{7,8,12,16–27} However, for others such as plasmonic wave guides, sensing and formation of percolation networks to optimize electrical and mechanical properties, end-to-end assembly is required to enable a locally enhanced field, efficient propagation of plasmons,^{28–33} or a pathway for carrier percolation.^{2,34} However, high aspect ratio NRs often have phase behavior similar to liquid crystals, where side-to-side assemblies are more energetically favorable in the absence of external guidance.¹⁰ Selective chemical modification of the ends of the NRs, albeit synthetically nontrivial, is perhaps among the most successful approaches toward the creation of long chains of end-to-end NR assembly.^{21,29}

Prefabricated templates^{35,36} or structural frameworks formed from the self-assembly of a block copolymer (BCP)³⁷ have been used to confine spherical nanoparticles or NRs to form one-dimensional (1D) or two-dimensional (2D) arrays. BCP-based supramolecules are effective in this as well.^{38,39} Geometric confinement imposed by the supramolecular framework leads to NR assembly in bulk. In cylindrical supramolecular nanocomposites, the high aspect ratio NRs are selectively sequestered at the interstitial sites between the BCP cylinders.³⁸

However, there have been limited successes in obtaining well-defined NR assemblies in thin films,^{25,36,37} especially with end-to-end NR arrangement over macroscopic distance. Directed coassembly of NRs and BCPs in thin films requires further consideration of a variety of parameters, as the presence of the substrate–film and film–air interfaces changes the energetic landscape and kinetic pathway of the assembly process. In thin films, the change in free energy upon incorporation of NRs can be expressed as $\Delta G = (\Delta H_{\text{surface}} + \Delta H_{\text{ligand-polymer}}) - T(\Delta S_{\text{con}} + \Delta S_{\text{trans}} + \Delta S_{\text{geometric}}) + (\Delta G_{\text{p-p}} - T\Delta S_{\text{orient}})$, where the first two groups of terms are similar to the free energy contributions considered for nanocomposites containing spherical nanoparticles.⁴⁰ Briefly, the first group of terms represents contributions from the surface tensions, and the nanoparticle ligand–polymer interaction. The second group accounts for the entropic changes upon nanoparticle incorporation originating from the conformational change of the polymer chain, the translational entropy of the nanoparticles, and the geometric chain packing of polymer chain, respectively. The last group of terms encompasses additional energetic contributions due to the anisotropy of the NRs and applies to NR nanocomposites in both bulk form and in thin films.³⁸ The particle–particle interaction, $\Delta G_{\text{p-p}}$, favors side-to-side NR assembly due to the dipole–dipole attraction and the depletion attraction.⁸ The orientational entropy of the NRs, ΔS_{orient} , accounts for the entropy originating from the anisotropic shape of NR. For NR nanocomposites, ΔS_{con} depends on the NR orientation and can be modulated by varying the morphology of supramolecular framework.³⁸ The geometric confinement from the supramolecular framework not

Received: July 31, 2013

Revised: August 27, 2013

Published: September 3, 2013

only controls NR location but also NR orientation. As shown in bulk,³⁸ the NR assembly upon blending with supramolecule mainly reflects the energetic competition between ΔG_{p-p} and ΔS_{con} .

For thin films, similar to what has been shown previously in nanocomposites containing spherical nanoparticles,^{40,41} the low surface tension of the NR and the entropy associated with polymer chain deformation upon particle incorporation must be balanced to prevent surface aggregation of NRs. For cylindrical supramolecular nanocomposites, nanoparticles larger than the interstitial sites between BCP cylinders are expelled to the film surface.⁴⁰ The long axis of NRs are generally several times the critical particle diameter and could be entropically excluded from the film interior to form aggregates on the surface. This also emphasizes the importance of the orientation dependence of ΔS_{con} , that is, NRs must assemble end-to-end in a cylindrical nanocomposite for it to be energetically favorable to sequester NRs in the interior of film.

Equally important to the energetic consideration above, the presence of NRs in the system can have drastic effects on the kinetics of assembly.^{42–46} Addition of NRs increase the viscosity of the composite⁴⁷ and may lead to kinetically trapped states rather than achieving equilibrium structures.⁴³ The probability of kinetic jamming effects appearing increases in nanocomposites containing high aspect ratio NRs and/or a high loading of NRs. Slowing or arrest of the system during the assembly process results in reduced grain sizes⁴⁴ and increased defect concentration.⁴⁵ Kinetic trapping may also prevent the coassembly of NRs and supramolecule even though the NR assembly is energetically favorable.

Here, 3D assembly of NRs in thin films upon blending with cylindrical supramolecules was investigated. End-to-end assemblies of NRs, 40 and 60 nm in length and ~ 5 nm in diameter, can be obtained in thin films using solvent annealing at moderate NR loading (3–6 vol %). When NR loading is beyond the capacity of the interstitial sites of cylindrical supramolecule, the NRs assembled side-to-side on the film surface. Furthermore, the assembly kinetics strongly depend on the NR loading and aspect ratio for NRs with a high aspect ratio, that is, 40 and 60 nm NRs, but not for the 20 nm NRs. Present studies provide useful guidance to achieve end-to-end NR assembly in thin films to suit needs for different NR-based applications.

The supramolecule, PS(19)-b-P4VP(5.2)(PDP)_{1,7}, is based on polystyrene (19 kDa)-block-poly(4-vinylpyridine) (5.2 kDa) (PS-b-P4VP) BCP and 3-pentadecylphenol (PDP) and constructed as shown previously.^{40,48,49} In thin films, it forms a cylindrical morphology where parallel PS cylinders are embedded in the P4VP(PDP)_{1,7} matrix. The PS cylinders are packed in a distorted hexagonal lattice and the NPs, passivated with alkyl ligands, are selectively sequestered in the interstitial region between PS cylinders. The use of P4VP(PDP)_{1,7} comb blocks rather than a typical coil polymer block increases the energy required for the deformation of the polymer chain and improves the geometric confinement of the nanorods within the matrix composed of the comb block. Figure 1a schematically shows one hypothetical coassembly, where NRs localize in the same location as the spherical particles⁴¹ and form end-to-end arrays.

All NRs are ~ 4 – 6 nm in diameter, comparable to that of spherical nanoparticles that are sequestered at the interstitial region between PS cylinders.⁴⁰ CdS NRs (60 nm in length) or CdSe/CdS seeded NRs (20 or 40 nm in length) capped with

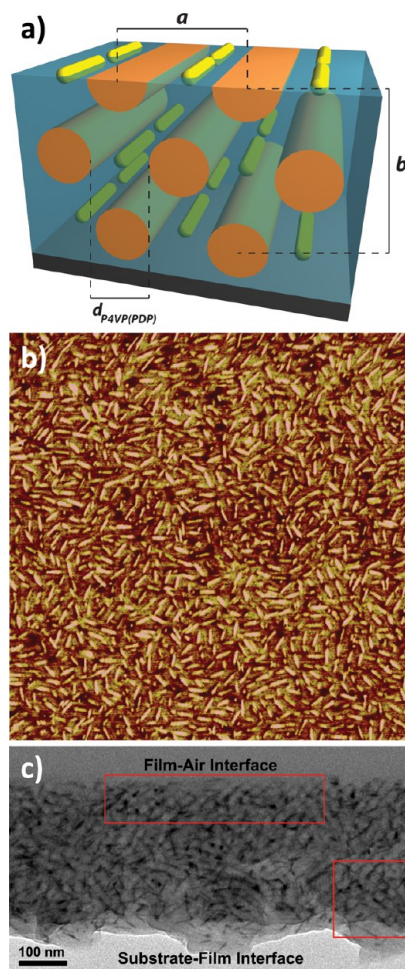


Figure 1. (a) A schematic of composite nanostructure. In this schematic, the PS domain is orange, the P4VP(PDP)_{1,7} domain is teal, and the nanorods are yellow. (b) AFM phase image of a 120 nm nanocomposite film with a 6% by volume loading. AFM image is $1 \mu\text{m} \times 1 \mu\text{m}$. (c) A cross-sectional TEM image of a film with 6% by volume 40 nm nanorods in which the P4VP(PDP)_{1,7} domain has been stained with iodine. Nanorods (black) can be seen dispersed in the P4VP(PDP)_{1,7} regions. The red boxed regions indicate areas where the BCP cylindrical microdomain is perpendicular to the viewing plane.

alkylphosphonic acids were used. The NR lengths were selected to tailor the degree of confinement imposed by the supramolecular structure on the NR arrangement. The 20 nm NRs are slightly shorter than the edge-to-edge distance between two PS cylinders, that is, $d_{P4VP(PDP)}$ (see Figure 1a) so that the NRs have more rotational freedom than longer NRs within the P4VP(PDP) matrix. Both the 40 and 60 nm NRs will encounter geometric confinement and it is energetically favorable to align the NRs parallel to PS cylinders in an end-to-end fashion. Furthermore, comparison between the nanocomposites based on 60 nm vs 40 NRs will provide insights to evaluate the effects of ΔG_{p-p} and kinetic jamming effects.

Figure 1b shows an AFM phase image of a solvent annealed ~ 120 nm thin film nanocomposite containing 6 vol % of 40 nm CdSe/CdS seeded NRs. The NRs are selectively sequestered within the P4VP(PDP)_{1,7} microdomains (dark regions) and oriented parallel to the surface. There is no aggregation of NRs on the surface even though the NR length is significantly larger than the diameter of spherical nanoparticles that are expelled

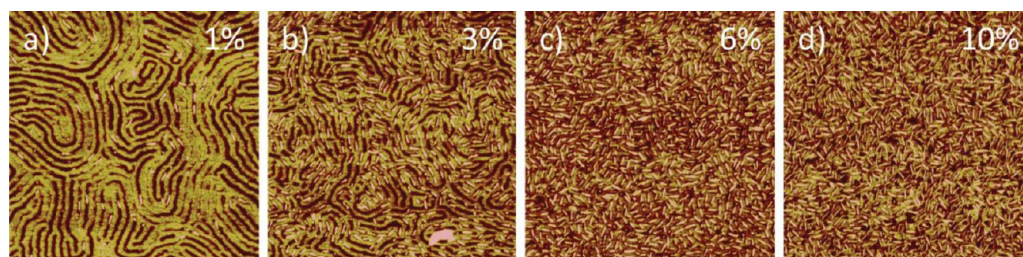


Figure 2. Representative AFM phase images of thin films of a blend of PS-b-P4VP(PDP)_{1.7} and 40 nm nanorods as a function of nanorod concentration. Nanorod volume fractions are (a) 1, (b) 3, (c) 6, and (d) 10%. AFM images are $1\ \mu\text{m} \times 1\ \mu\text{m}$.

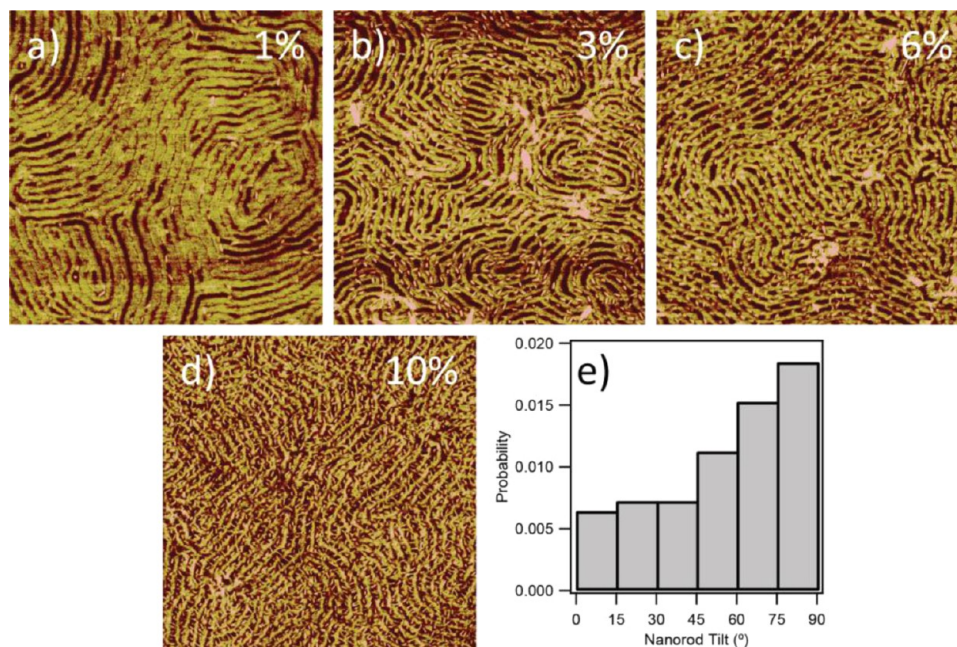


Figure 3. Representative AFM phase images of thin films of a blend of PS-b-P4VP(PDP)_{1.7} and 20 nm nanorods as a function of nanorod concentration. Nanorod volume fractions are (a) 1, (b) 3, (c) 6, and (d) 10%. (e) Histogram of the angle between the long axis of the NRs and the PS cylinders in (d). AFM images are $1\ \mu\text{m} \times 1\ \mu\text{m}$.

from the interior of thin film ($\sim 10\ \text{nm}$).⁴⁰ Figure 1c shows the cross-sectional TEM image of the same film. NRs that are well dispersed in the interior of film can be clearly seen. The NRs primarily segregate to the interstitial sites between four PS cylinders, forming a distorted hexagonal lattice. However, the lattice order (highlighted regions of Figure 1c) only persists over a short distance (the grain size is on the order of 100 nm) and there are a large number of defects. This poor long-range order can be attributed to the kinetics of assembly. The long axis of the NRs is substantially larger than the spherical NPs, so the NRs diffuse through the system more slowly. The inclusion of these large particles can also slow the diffusion of the supramolecule, causing a reduction in the grain size. Nevertheless, the 3D assemblies of NRs in the thin film suggest that under the solvent annealing condition used here, $\Delta G_{\text{p-p}}$ and $\Delta H_{\text{surface}}$ are not large enough to overcome the energetic contributions sequestering NRs within the P4VP(PDP)_{1.7} microdomains. For the rest of studies, we focus on AFM studies to investigate NR assemblies.

The concentration of NRs affects the entropic factors ΔS_{con} and ΔS_{trans} and has a significant effect on the kinetics of assembly. Figure 2 shows the AFM images of thin films of 40 nm NR supramolecular nanocomposite with the NR volume fractions, f_{NR} , ranging from 1 to 10 vol %. For all samples, the

NRs are embedded in the film and there is no preferential surface aggregation of NRs. At a f_{NR} of 3 vol %, NRs with end-to-end arrangement can be clearly seen. While NRs only assemble in close proximity to each other frequently at $f_{\text{NR}} = 6$ vol %, alignment parallel to the PS cylindrical microdomains is excellent even at lower loading rates. However, at $f_{\text{NR}} = 10$ vol %, the NRs cover a large fraction of the surface and the NRs begin assembling side-to-side. As the f_{NR} increases, the grain size of the supramolecular microdomains decreases from a 0.5–1 μm at a NR loading of 1 vol % to 50–100 nm at 10 vol %.

The NR length affects energetic contributions, including $\Delta G_{\text{p-p}}$, ΔS_{orient} and ΔS_{con} . For shorter NRs, the geometric restrictions from the supramolecular framework may be diminished and $\Delta G_{\text{p-p}}$ becomes weaker. Reducing the NR length also allows for faster diffusion and accelerates the assembly process. To investigate these effects, 20 nm long NRs were used. The NRs are shorter than $d_{\text{P4VP(PDP)1.7}}$, the width of the P4VP(PDP)_{1.7} microdomains (see Figure 1a). The angular distribution of the 20 nm nanorods in Figure 3d was determined by measuring the angle of the long axis of the nanorods relative to the microdomain they reside in using ImageJ. Nanorods whose orientation relative to the microdomain was not clear were skipped. Histograms were calculated with this data using the built-in histogram functionality in Igor

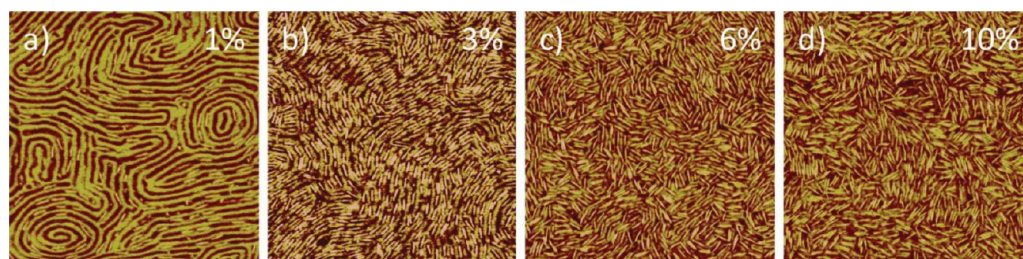


Figure 4. Representative AFM phase images of thin films of a blend of PS-b-P4VP(PDP)_{1.7} and 60 nm nanorods as a function of nanorod concentration. Nanorod volume fractions are (a) 1, (b) 3, (c) 6, and (d) 10%. AFM images are $1\ \mu\text{m} \times 1\ \mu\text{m}$.

Pro. As shown in Figure 3e, the NRs reside within P4VP(PDP)_{1.7} microdomains at angles ranging between 0° to 90° relative to the PS cylinders, weighted toward 90° . Though the 20 nm NRs do not assemble end-to-end for the range of f_{NR} investigated, they also do not demonstrate side-to-side assembly, even at 10 vol %, where they occupy a large fraction of the surface. Furthermore, the grain size remains similar up to a NR loading of 10 vol %, showing that the addition of shorter NRs has minimal effect on the assembly kinetics of nanocomposite thin films.

Figure 4 shows the AFM images of thin films of nanocomposites containing 60 nm CdS. The 60 nm NRs are significantly longer than $d_{\text{P4VP(PDP)}}$ and are subject to more geometric restrictions than the 40 nm NRs. In addition, as $\Delta G_{\text{p-p}}$ scales with particle volume, the interparticle attractive forces are significantly stronger for 60 nm NRs than for 40 nm NRs. The NRs remain completely within the P4VP(PDP)_{1.7} microdomains, assembling end-to-end at 3 vol % due to the geometric restrictions imposed on the NRs. As with the 40 nm NRs, the grain size of the nanocomposite decreases as f_{NR} increases. At 10 vol %, the grain size is less than 100 nm, not much larger than the length of a NR. However, at 3 vol %, it remains comparable to the grain size seen at a 1 vol % loading, while the NR concentration remains sufficiently high to allow end-to-end assembly.

The results reflect the energetic competition between $\Delta G_{\text{p-p}}$ and the entropic contributions ΔS_{con} and ΔS_{trans} involved in the assembly of the NR nanocomposites. $\Delta G_{\text{p-p}}$ is quite small for the 20 nm NRs and side-to-side assembly is almost absent. As both the dipole of the particles and the strength of the depletion attraction decrease with a smaller particle volume, this is reasonable. The 20 nm NRs are also less affected by the geometric restrictions in comparison to longer NRs and do not necessarily assemble end-to-end parallel to the microdomains. For these short rods, the polymer chain deformation required to accommodate their off-axis assembly is not as severe as that required by the longer NRs, reducing the ΔS_{con} associated with incorporating NRs that do not lie parallel to the cylindrical microdomains. Their orientational entropy ΔS_{orient} therefore outweighs the reduced entropic penalty for chain deformation. For the longer 40 and 60 nm rods, the geometric restriction imposed by the supramolecule through ΔS_{con} is clearly visible; the NRs lie parallel to the microdomains. The assembly at a low loading rate indicates that the driving forces for the NRs to assemble side-to-side, $\Delta G_{\text{p-p}}$, are weaker than the driving forces for the NRs to assemble within the microdomains. However, as the loading rate increases, the translational entropy of the NRs ΔS_{trans} becomes a less important factor, and the energetic gains from assembling side-to-side are larger than the entropic penalties associated with deforming the supramolecule chains ΔS_{con} . Thus, the NRs begin assembling side-to-side once past a

critical $f_{\text{NR}} - 6$ vol % for 40 nm NRs and 3 vol % for 60 nm NRs.

The kinetic impact of NR size and concentration plays a key role and requires more consideration than that of nanocomposites containing spherical nanoparticles. The smaller size of the 20 nm NRs causes them to exhibit limited to no effect on the kinetics of assembly at the concentrations investigated here. In contrast, the kinetic effects of the longer NRs can be deduced from the decrease in grain size observed. Though no evidence of a fully kinetically trapped state is apparent, the trend of reduced grain size at higher loading rates is evident. Since the ordering of supramolecular assemblies requires material transport, the addition of these relatively large, slowly diffusing NRs in turn slows the reorientation and defect elimination of the supramolecular microdomains, causing the nanocomposites to exhibit reduced grain sizes with increased volume fractions of NRs.

In summary, we have investigated the coassembly of a BCP-based supramolecule and NRs of various lengths and at various loading rates in a thin film morphology. Nanorods with aspect ratio of 8–12 can be aligned in an end-to-end fashion in thin films by imposing geometric confinement via supramolecular assembly. End-to-end NR assembly over large areas without significant reduction in grain size was achieved in two cases: a 3% by volume loading rate of 40 nm NRs, and a 3% by volume loading rate of 60 nm NRs. Assembly and orientation of the NRs in the film was dictated by a variety of energetic factors, of which $\Delta G_{\text{p-p}}$, ΔS_{con} , ΔS_{trans} , ΔS_{orient} and $\Delta H_{\text{ligand-polymer}}$ were explored in this work. The kinetics of assembly also played a large role. This becomes more prominent as the rods become larger and as the loading increases, limiting grain size. Because of the levels of swelling and time scales likely to be required to overcome this slow diffusion, achieving long-range order will require careful control to enable NR diffusion without causing film dewetting.

Methods. Sample Preparation. Block copolymers (PS-b-P4VP) were purchased from Polymer Source; PDP (95%) was purchased from Arcos. Chloroform (pentene stabilized) was purchased from Fisher. All chemicals were used as received. A detailed description of nanorod synthesis can be found in Supporting Information. PS-b-P4VP and PDP were dissolved separately in chloroform to form 1–2% w/v stock solutions. The PS-b-P4VP solution was then added dropwise in appropriate amounts to the PDP solution, followed by stirring overnight. Synthesized nanorods were suspended in chloroform at the same concentration as the supramolecule solution. The PS-b-P4VP(PDP)_{1.7} and nanorod solutions were mixed and used immediately. Thin films were prepared by spin-coating the mixed solutions on to silicon wafers at speeds ranging from 1000 to 3000 rpm. Sample thicknesses were measured using a Filmetrics F20 interferometer. Samples were annealed using

300–800 μL of CHCl_3 injected into a 250 mL top-capped jar at room temperature.

TEM. Thin films were spun-cast onto polystyrene-coated sodium chloride disks as they would be onto silicon wafers. After solvent annealing, films were floated off the substrate onto water and retrieved using a precured block of Araldite 502 epoxy (Electron Microscopy Sciences). The film was then cured at 60 °C for four hours. Thin sections ~ 60 nm in thickness were microtomed from the film using an RMC MT-X ultramicrotome (Boeckler Instruments) and picked up from water onto copper TEM grids. The thin sections were examined using an FEI Tecnai 12 at an accelerating voltage of 120 kV.

■ ASSOCIATED CONTENT

Supporting Information

Additional information and figures regarding nanorod synthesis and characterization. This material is available free of charge via the Internet at <http://pubs.acs.org>.

■ AUTHOR INFORMATION

Corresponding Author

*E-mail: tingxu@berkeley.edu.

Present Address

^{||}J.H.N. is currently affiliated with the Energy and Resources Group, University of California, Berkeley.

Author Contributions

The manuscript was written through contributions of all authors. All authors have given approval to the final version of the manuscript.

Notes

The authors declare no competing financial interest.

■ ACKNOWLEDGMENTS

This work was supported by the Department of Energy, Office of Basic Energy Science through the Organic/Inorganic Nanocomposites program under contract DE-AC02-05CH11231.

■ REFERENCES

- (1) Chun, J. Y.; Lee, J. W. *Eur. J. Inorg. Chem.* **2010**, *27*, 4251–4263.
- (2) Huynh, W. U.; Dittmer, J. J.; Alivisatos, A. P. *Science* **2002**, *295*, 2425–7.
- (3) Hore, M. J. A.; Composto, R. J. *ACS Nano* **2010**, *4*, 6941–9.
- (4) Stebe, K. J.; Lewandowski, E.; Ghosh, M. *Science* **2009**, *325* (5937), 159–160.
- (5) Bockstaller, M. R.; Mickiewicz, R. A.; Thomas, E. L. *Adv. Mater.* **2005**, *17*, 1331–1349.
- (6) Nie, Z.; Petukhova, A.; Kumacheva, E. *Nat. Nanotechnol.* **2010**, *5*, 15–25.
- (7) Glotzer, S. C.; Solomon, M. J. *Nat. Mater.* **2007**, *6*, 557–62.
- (8) Baker, J. L.; Widmer-Cooper, A.; Toney, M. F.; Geissler, P. L.; Alivisatos, A. P. *Nano Lett.* **2010**, *10*, 195–201.
- (9) Ghezelbash, A.; Koo, B.; Korgel, B. A. *Nano Lett.* **2006**, *6*, 1832–1836.
- (10) Li, L.-S.; Alivisatos, A. P. *Adv. Mater.* **2003**, *15*, 408–411.
- (11) Nikoobakht, B.; Wang, Z. L.; El-Sayed, M. A. *J. Phys. Chem. B* **2000**, *104* (36), 8635–8640.
- (12) Ryan, K. M.; Mastroianni, A.; Stancil, K. A.; Liu, H.; Alivisatos, A. P. *Nano Lett.* **2006**, *6*, 1479–1482.
- (13) Hammond, M. R.; Dietsch, H.; Pravaz, O.; Schurtenberger, P. *Macromolecules* **2010**, *43* (20), 8340–8343.
- (14) Vallooran, J. J.; Bolisetty, S.; Mezzenga, R. *Adv. Mater.* **2011**, *23* (34), 3932–3937.
- (15) Mauter, M. S.; Elimelech, M.; Osuji, C. O. *ACS Nano* **2010**, *4* (11), 6651–6658.
- (16) Murphy, C. J.; Orendorff, C. J. *Adv. Mater.* **2005**, *17*, 2173–2177.
- (17) Gupta, S.; Zhang, Q.; Emrick, T.; Russell, T. P. *Nano Lett.* **2006**, *6*, 2066–9.
- (18) Li, L.-S.; Walda, J.; Manna, L.; Alivisatos, A. P. *Nano Lett.* **2002**, *2*, 557–560.
- (19) Titov, A. V.; Král, P. *Nano Lett.* **2008**, *8*, 3605–12.
- (20) Li, L. S.; Marjanska, M.; Park, G. H. J.; Pines, A.; Alivisatos, A. P. *J. Chem. Phys.* **2004**, *120* (3), 1149–1152.
- (21) Fava, D.; Nie, Z.; Winnik, M. A.; Kumacheva, E. *Adv. Mater.* **2008**, *20*, 4318–4322.
- (22) Jang, S. G.; Kramer, E. J.; Hawker, C. J. *J. Am. Chem. Soc.* **2011**, *133*, 16986–96.
- (23) Jones, M. R.; Macfarlane, R. J.; Lee, B.; Zhang, J.; Young, K. L.; Senesi, A. J.; Mirkin, C. A. *Nat. Mater.* **2010**, *9*, 913–7.
- (24) Liu, J.; Wang, L.; Sun, X.; Zhu, X. *Angew. Chem., Int. Ed.* **2010**, *49*, 3492–5.
- (25) Ploshnik, E.; Salant, A.; Banin, U.; Shenhar, R. *Adv. Mater.* **2010**, *22*, 2774–2779.
- (26) Rycenga, M.; McLellan, J. M.; Xia, Y. *Adv. Mater.* **2008**, *20*, 2416–2420.
- (27) Yan, L. T.; Popp, N.; Ghosh, S. K.; Boker, A. *ACS Nano* **2010**, *4* (2), 913–920.
- (28) Chen, D. L.; Gao, L. *J. Cryst. Growth* **2004**, *264* (1–3), 216–222.
- (29) Thomas, K. G.; Barazzouk, S.; Ipe, B. I.; Joseph, S. T. S.; Kamat, P. V. *J. Phys. Chem. B* **2004**, *108* (35), 13066–13068.
- (30) Jain, P. K.; Eustis, S.; El-Sayed, M. A. *J. Phys. Chem. B* **2006**, *110* (37), 18243–18253.
- (31) Wang, L.; Zhu, Y.; Xu, L.; Chen, W.; Kuang, H.; Liu, L.; Agarwal, A.; Xu, C.; Kotov, N. A. *Angew. Chem., Int. Ed.* **2010**, *49* (32), 5472–5475.
- (32) Zhong, L.; Zhou, X.; Bao, S.; Shi, Y.; Wang, Y.; Hong, S.; Huang, Y.; Wang, X.; Xie, Z.; Zhang, Q. *J. Mater. Chem.* **2011**, *21* (38), 14448.
- (33) Zhu, Y.; Kuang, H.; Xu, L.; Ma, W.; Peng, C.; Hua, Y.; Wang, L.; Xu, C. *J. Mater. Chem.* **2012**, *22* (6), 2387.
- (34) Buxton, G. A.; Balazs, A. C. *Mol. Simul.* **2004**, *30*, 249–257.
- (35) Nepal, D.; Onses, M. S.; Park, K.; Jespersen, M.; Thode, C. J.; Nealey, P. F.; Vaia, R. A. *ACS Nano* **2012**, *6* (6), 5693–5701.
- (36) Zhang, Q.; Gupta, S.; Emrick, T.; Russell, T. P. *J. Am. Chem. Soc.* **2006**, *128* (12), 3898–3899.
- (37) Deshmukh, R. D.; Liu, Y.; Composto, R. J. *Nano Lett.* **2007**, *7*, 3662–8.
- (38) Thorkelsson, K.; Mastroianni, A. J.; Ercius, P.; Xu, T. *Nano Lett.* **2012**, *12*, 498–504.
- (39) Li, W.; Zhang, P.; Dai, M.; He, J.; Babu, T.; Xu, Y.-L.; Deng, R.; Liang, R.; Lu, M.-H.; Nie, Z.; Zhu, J. *Macromolecules* **2013**, *46* (6), 2241–2248.
- (40) Kao, J.; Bai, P.; Lucas, J. M.; Alivisatos, A. P.; Xu, T. *J. Am. Chem. Soc.* **2013**, *135*, 1680–3.
- (41) Kao, J.; Bai, P.; Chuang, V. P.; Jiang, Z.; Ercius, P.; Xu, T. *Nano Lett.* **2012**, *12*, 2610–8.
- (42) Chung, H. J.; Taubert, A.; Deshmukh, R. D.; Composto, R. J. *Europhys. Lett.* **2004**, *68* (2), 219–225.
- (43) Li, L.; Miesch, C.; Sudeep, P. K.; Balazs, A. C.; Emrick, T.; Russell, T. P.; Hayward, R. C. *Nano Lett.* **2011**, *11*, 1997–2003.
- (44) Yurekli, K.; Karim, A.; Amis, E. J.; Krishnamoorti, R. *Macromolecules* **2003**, *36* (19), 7256–7267.
- (45) Peng, G. W.; Qiu, F.; Ginzburg, V. V.; Jasnow, D.; Balazs, A. C. *Science* **2000**, *288* (5472), 1802–1804.
- (46) Yan, L.-T.; Xie, X.-M. *Prog. Polym. Sci.* **2013**, *38* (2), 369–405.
- (47) Brown, E.; Forman, N. A.; Orellana, C. S.; Zhang, H. J.; Maynor, B. W.; Betts, D. E.; DeSimone, J. M.; Jaeger, H. M. *Nat. Mater.* **2010**, *9* (3), 220–224.

(48) Ruokolainen, J.; Saariaho, M.; Ikkala, O.; ten Brinke, G.; Thomas, E. L.; Torkkeli, M.; Serimaa, R. *Macromolecules* **1999**, *32*, 1152–1158.

(49) Valkama, S.; Ruotsalainen, T.; Nykänen, A.; Laiho, A.; Kosonen, H.; ten Brinke, G.; Ikkala, O.; Ruokolainen, J. *Macromolecules* **2006**, *39*, 9327–9336.